

Retinotopic Organization of the Primary Visual Cortex of Flying Foxes (*Pteropus poliocephalus* and *Pteropus scapulatus*)

MARCELLO G.P. ROSA, LEISA M. SCHMID, LEAH A. KRUBITZER,
AND JOHN D. PETTIGREW

Vision, Touch and Hearing Research Centre, Department of Physiology and Pharmacology,
The University of Queensland, St. Lucia QLD 4072, Australia

ABSTRACT

The representation of the visual field in the occipital cortex was studied by multiunit recordings in seven flying foxes (*Pteropus* spp.), anesthetized with thiopentone/N₂O and immobilized with pancuronium bromide. On the basis of its visuotopic organization and architecture, the primary visual area (V1) was distinguished from neighboring areas. Area V1 occupies the dorsal surface of the occipital pole, as well as most of the tentorial surface of the cortex, the posterior third of the mesial surface of the brain, and the upper bank of the posterior portion of the splenial sulcus. In each hemisphere, it contains a precise, visuotopically organized representation of the entire extent of the contralateral visual hemifield. The representation of the vertical meridian, together with 8–15° of ipsilateral hemifield, forms the anterior border of V1 with other visually responsive areas. The representation of the horizontal meridian runs anterolateral to posteromedial, dividing V1 so that the lower visual quadrant is represented medially, and the upper quadrant laterally. The total surface area of V1 is about 140 mm² for *P. poliocephalus*, and 110 mm² for *P. scapulatus*. The representation of the central visual field is greatly magnified relative to that of the periphery. The cortical magnification factor decreases with increasing eccentricity, following a negative power function. Conversely, receptive field sizes increase markedly with increasing eccentricity, and therefore the point-image size is approximately constant throughout V1. The emphasis in the representation of the area centralis in V1 is much larger than that expected on the basis of ganglion cell counts in flat-mounted retinas. Thus, a larger degree of convergence occurs at the peripheral representations in the retino-geniculo-cortical pathway, in comparison with the central representations. The marked emphasis in the representation of central vision, the wide extent of the binocular field of vision, and the relatively large surface area of V1 reflect the importance of vision in megachiropterans. © 1993 Wiley-Liss, Inc.

Key words: megachiroptera, vision, cortical magnification factor, striate cortex, evolution

The mammalian order Chiroptera is composed of two distinct suborders, Microchiroptera and Megachiroptera. Several anatomical, physiological, biogeographical, and behavioral characteristics (recently reviewed by Pettigrew et al., '89) differentiate these groups. Of special interest to sensory neurophysiologists, however, is the fact that members of these two taxa, which together comprise all flying mammals, have adapted to use different sensory modalities as their main means of navigation, obstacle avoidance, and food gathering. Microchiropterans are adapted (to different degrees) to the use of echolocation by means of a specialized sound-emitting laryngeal sonar and by several exquisite adaptations in the central nervous system (see Suga, '89, for a review). Megachiropterans, on the other hand, generally rely on vision, with the exception of a cave-dwelling

species that seems to have independently evolved a primitive type of sonar (Novick, '58; Neuweiler, '62; Wimsatt, '70).

In general, the study of the sensory systems of chiropterans presents some interesting questions related to the specific adaptations that might have occurred in relation to the evolution of flight. Presently, much is known about the anatomy and physiology of the auditory pathways of several species of microchiropterans (e.g., Suga, '89; Neuweiler, '90; Covey and Casseday, '91). Studies of the somatosensory and motor pathways in both suborders have likewise progressed by the application of modern electrophysiological and anatomical tracer techniques (Calford et al., '85,

Accepted February 22, 1993.

Wise et al., '86; Kennedy, '91; Krubitzer and Calford, '92; Krubitzer et al., '93). However, a major gap remains in our knowledge of the visual system of bats. Some reports have addressed the physiological optics, the organization of the retina, and the retinofugal projections (Neuweiler, '62; Cotter and Pentney, '79; Cotter, '81, '85; Pentney and Cotter, '81; Pettigrew, '86; Graydon et al., '87; Pettigrew et al., '88; Reimer, '89; Dann and Buhl, '90; Thiele et al., '91), but nothing is known about the physiology of the chiropteran visual cortex.

Here, we will describe the retinotopic organization of the primary visual cortex (area 17, or V1) in two closely related species of megachiropterans, the little red flying fox (*Pteropus scapulatus*) and the grey-headed flying fox (*Pteropus poliocephalus*). These bats are "typical" representatives of Megachiroptera, in that they use vision as the primary means of orientation during flight. They share the same classes of ganglion cells found in the carnivore retina, and their visual acuity at scotopic levels of illumination rivals that of cats and humans (Graydon et al., '87; Pettigrew et al., '88; Dann and Buhl, '90). Interestingly, their retinotectal pathway is specialized in a manner similar to that observed among primates: the projection of the visual field to the superior colliculus is restricted to the contralateral hemifield (Pettigrew, '86). A comprehensive behavioral study of the visual capacities of another member of this genus, *Pteropus giganteus*, has also been published (Neuweiler, '62). In the present investigation, a precise representation of the contralateral hemifield was observed in V1, and quantified in terms of its magnification factors and receptive-field sizes. A preliminary report of these data has also been published in abstract form (Rosa et al., '92b).

MATERIALS AND METHODS

Seven adult male flying foxes (four *P. poliocephalus* weighing 580–900 g; three *P. scapulatus* weighing 320–500 g) were used for electrophysiological recordings. Four additional animals (two *P. poliocephalus*, two *P. scapulatus*) were used to determine the relationship between the optic disc and the visual field meridians, by means of ganglion cell counts in flat-mounted retinas.

Animal care and preparation

Each flying fox underwent a single, non-recovery recording session. Initially, the animal was tranquilized with benzodiazepines (Valium, 1.5 mg/kg IM) and received IM injections of atropine (0.15 mg/kg) and dexamethasone (0.4 mg/kg); shortly after, it was anesthetized with a mixture of ketamine (50 mg/kg) and xylazine (5 mg/kg). After the disappearance of all signs of withdrawal reflexes, the animal was submitted to a tracheotomy, and a cannula 3–3.5 mm in diameter was inserted in order to allow for artificial ventilation. The flying fox was then transferred to a

stereotaxic frame, where the implantation surgery was performed. Both the left and right veins running in the occipitopollicalis muscles (at the anterior edge of the propatagia) were cannulated in order to allow for intravenous injections. Throughout the subsequent surgical procedures and experimental sessions, the animal lay on a thermostatically controlled soft heating pad, and the electrocardiogram was continuously monitored by D2 derivation by means of a virtual oscilloscope system (Scope v3.2.5), run with the aid of a MacLab/8 (Analog Digital Instruments) and an Apple Macintosh LC computer. The electroencephalogram was also monitored during two of the initial experiments; however, the heart rate was found to provide a reliable physiological measure of anesthetic state, and was used alone in the remaining cases. The heart rate of an anesthetized flying fox was found to vary between 180 and 240 beats/min, and additional doses of anesthetic (thiopentone sodium 10 mg/kg IV) were given whenever the rate accelerated beyond the normal rate. The implant consisted of a bolt to hold the head to the arm of a custom-made stereotaxic head holder and an acrylic well, anchored to the skull by small orthopedic screws in a dental acrylic base. A craniotomy 10–15 mm in diameter was made in the region circumscribed by the well, the dura-mater was resected, and the surface of the cortex was covered with oil. A photograph of the cortical surface was then taken to be used as reference for the placement of electrode penetrations. Once the surgical procedures were completed, the eye, mouth, and ear bars were removed, and the head was held in position only by the implanted bolt. The modified stereotaxic head holder allowed for head rotation along all axes, and offered an almost unobstructed field of vision. Finally, muscular paralysis was induced by the intravenous infusion of pancuronium bromide (Pavulon, 0.15 mg/kg, followed by 0.15 mg/kg/hr) in a saline solution with glucose (1.2%) and dexamethasone (0.4 mg/kg/hr). The animal was subsequently maintained under artificial ventilation with a gaseous mixture of nitrous oxide/oxygen (7:3), and the respiratory volume and rate were adjusted in order to keep the percentage of CO₂ in the expired air between 3.8 and 4.5%. Additional doses of thiopentone were administered as needed during the experiments, in order to keep the heart rate within the above specified limits. The experimental sessions were 12–24 hr long.

Protection of the cornea, dioptric correction, and control for eye movements

Mydriasis and cycloplegia were induced by the topical application of atropine (1%) and phenylephrine hydrochloride (10%) eye drops. The right eye was focused on the surface of a 40-cm-radius translucent hemispheric screen by means of an appropriate hard contact lens (curvature radius 4.5–4.9 mm), selected by slit retinoscopy. This lens also protected the cornea from desiccation, and the quality of the optic media seemed to be kept stable during the experiment, as evaluated by repeated ophthalmoscopic inspections. The left eye was kept covered. The position of the optic disc was projected onto the hemispheric screen by means of a reversible ophthalmoscope at the beginning of the recordings, and then checked several times during the experiment. In every instance, two independent observations were made by different investigators, and the estimates of the position of the center of the optic disc never differed by more than 5°. The movement of the eyes during

Abbreviations

CMF	cortical magnification factor
ecc	eccentricity
HM	horizontal meridian
OD	optic disc
PS	area prostriata
RF	receptive field
V1	primary visual area
V2	second visual area
VM	vertical meridian

the sessions never exceeded 10° in amplitude, and this slow drift was taken into account in the posterior data analysis.

Recordings

Tungsten in glass microelectrodes with an exposed tip of 10–15 μm (impedance 2–3 $\text{M}\Omega$ at 1 kHz) were inserted in the parasagittal plane, at different angles from the vertical for each animal. In a typical experiment, recording sites along a penetration were separated by approximately 400 μm , and the penetrations were no less than 500 μm apart. The experiment in case PP1 was especially designed to explore the extent of the ipsilateral representation at the V1/V2 border (Payne, '90), and therefore a finer grid (recordings every 100–200 μm) was adopted. In each site, luminous white spots and bars were moved on the surface of the screen by means of a hand-held projector, and the minimum response fields of small unit clusters were mapped by correlating the stimulation of specific portions of the visual field with the increments of the neural activity, as monitored both on an oscilloscope and through an audio system. All stimulation was done under scotopic conditions. Small electrolytic lesions (4 μA , 10–15 sec, electrode negative) were placed in several penetrations, to aid in the post mortem track reconstruction and identification of the recording sites.

Histology

At the end of the experiment, the animal was sacrificed by means of a lethal dose of sodium pentobarbital (50 mg/kg) and transcardially perfused with 0.9% saline, followed by 4% paraformaldehyde in 0.1 M phosphate buffer and 4% paraformaldehyde/10% sucrose in phosphate buffer. In most cases, the brain was removed from the skull, blocked in stereotaxic coordinates, and left overnight in the same fixative. These cases were sectioned at 40 μm in the parasagittal plane with the aid of a freezing microtome. In one case (PP3), the brain was flat-mounted by careful dissection as detailed previously (Krubitzer and Calford, '92) and sectioned parallel to the cortical surface. Every section was saved, and consecutive sections were histochemically stained for cytochrome oxidase (cytox; Wong-Riley, '79), stained for myelin by the Gallyas ('79) protocol or for cell bodies with cresyl violet. The reconstruction of the position of the recording sites was based on the location of the electrolytic lesions and transitions between the cortex and the white matter. An estimate of the shrinkage during the histological processing was obtained by comparing the real distance between penetrations (based on the microdrive readings) with the distance measured in the sections, and was found to vary between 12% and 20% (linearly) in different cases.

Unfolding of the cortical surface and visual maps

In order to obtain "maps" of the visual topography of V1 for each animal, we graphically unfolded the striate cortex and adjacent areas by means of Van Essen and Maunsell's ('80) technique. Contours of layer IV of parasagittal sections 800 μm apart were traced on paper and graphically "smoothed" keeping neighborhood relationships. In order to ensure the proper alignment and spacing between sections, we used horizontal reference needles as landmarks to align the sections, and calculated the correct spacing by trigonometry every 2 mm along each contour. We introduced discontinuities in the map whenever the surface

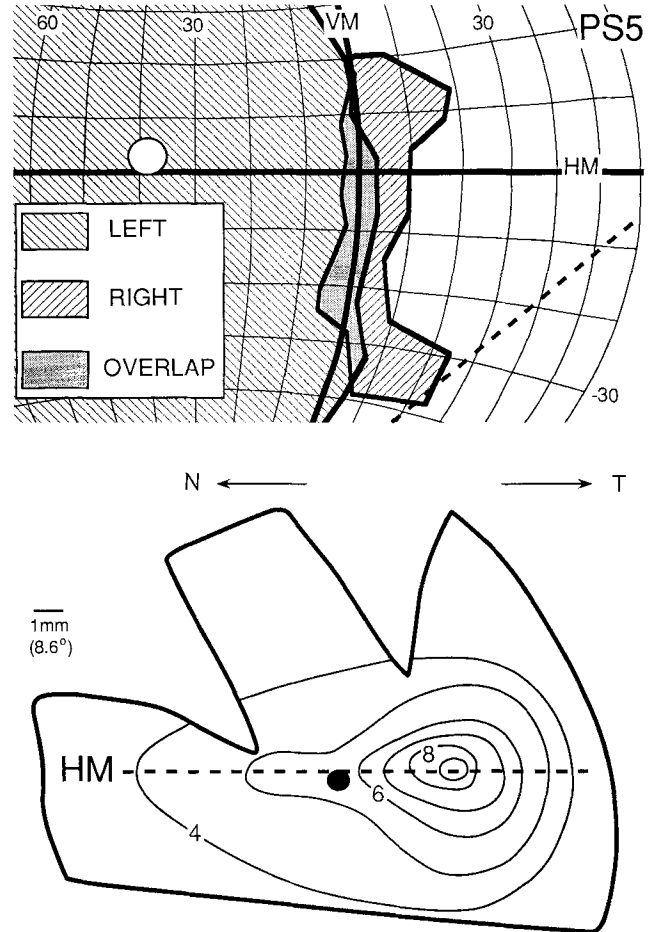


Fig. 1. Determination of the vertical and horizontal meridians of the visual field in flying foxes. **Upper:** Determination of the vertical meridian (VM) based on recordings across the V1/V2 boundary on the two hemispheres of a *P. scapulatus*. The diagram illustrates the central visual field in an equatorial-zenithal map similar to those shown in Figures 3 and 5. Azimuths and elevations are shown in 10° intervals. The envelopes containing the boundaries of the receptive fields recorded through stimulation of the right eye in the left and right hemispheres are shown with different diagonal patterns except in the region of overlap, which is shown in grey. The projection of the optic disc into the visual field is shown by the white circle, and the nasal border of the unocular field of vision is shown by the dashed line. The VM was estimated as a vertical line passing approximately through the center of the overlap zone. The VM forms an arch in this figure due to the rotation of the representation that we introduced in order to be able to illustrate azimuths larger than 90° (see Fig. 3). **Lower:** Determination of the horizontal meridian (HM) based on counts of ganglion cells in a Nissl-stained, flat-mounted retina of a *P. poliocephalus*. Isodensity profiles are shown as continuous lines; the values are thousands of ganglion cells/mm². The HM (dashed line) was assumed to be a line through the region of highest cell density, and parallel to the "visual streak." The optic disc is the black circle. N, nasal, T, temporal. The scale bar = 1 mm, or 8.6° in the visual field, according to Pettigrew ('86).

proved to be unflattenable, in order to keep the isometry. Examples of flat reconstructions are shown in Figures 4 and 6. The receptive field boundaries were recorded in terms of an equatorial-zenithal system, after compensation for the residual eye movements. Receptive field centers were calculated as the mean azimuth and elevation of their four corners, and the interpolated isoazimuth and isoeleva-

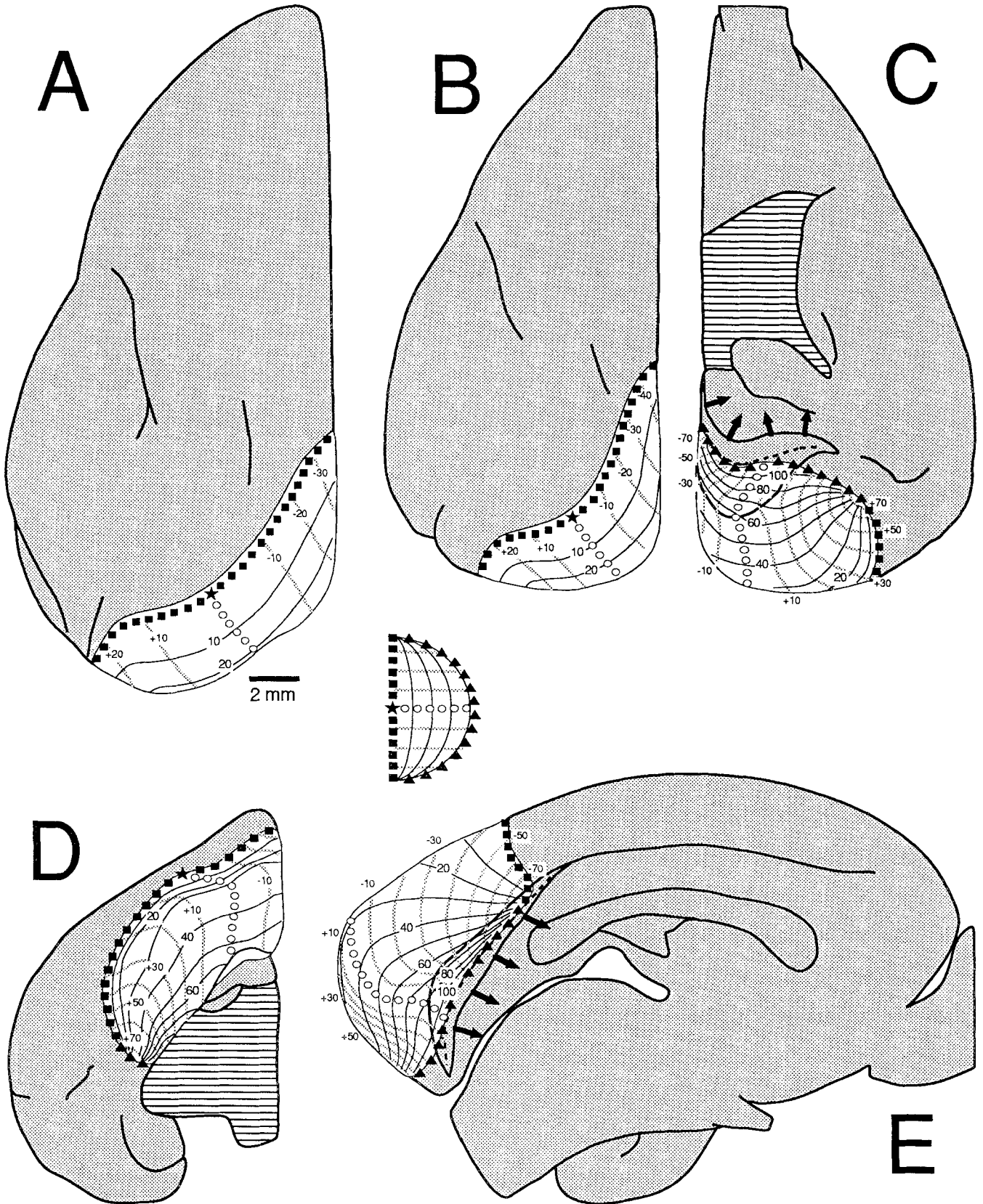


Figure 2

tion lines were hand-drawn in the flat reconstructions. Calculations of receptive field size and of the distance between field centers, for the magnification factors, took into account the distortion introduced at the visual field periphery by the equatorial-zenithal system, by first converting the coordinates to a spheric polar system (Gattass and Gattass, '75).

Determination of the axes of reference

Since the position of the area centralis of flying foxes cannot be established by ophthalmoscopic inspection, the relationship between the vertical (VM) and horizontal (HM) meridians and the optic disc (OD) was determined by electrophysiological recordings and by the examination of ganglion cell density contours in flat-mounted retinas. The position of the VM was determined independently for each case by recording receptive fields across the border between areas V1 and V2 in both hemispheres (Kaas et al., '70). As previously shown in other species (see Payne, '90, for a recent review), there is a strip of the visual field centered on the VM that is bilaterally represented. Thus, by recording several rows of recording sites in both hemispheres, a mean reversal point of the receptive field sequences can be calculated, and this is a precise estimate of the position of the VM (Fig. 1, upper). The mean distance between the VM and the OD was found to be 34.3° (range, $32\text{--}37.5^\circ$) in *P. poliocephalus*, and 37.5° ($36.5\text{--}39.5^\circ$) in *P. scapulatus*. The HM is defined as a perpendicular to the VM through the center of gaze. For the calculation of the mean position of the HM, seven flat-mounted retinas stained with cresyl violet (technique described by Pettigrew et al., '88), from four animals, were examined. The HM was considered as a line through the area centralis, parallel to the direction of the elongation of the isodensity contours (Fig. 1, lower). The angular distance between the HM line and the center of the optic disc was then calculated by using the retinal magnification factors for *P. poliocephalus* and *P. scapulatus* (Pettigrew, '86; Pettigrew et al., '88). On the average, the HM was found to be 3.0° (range, $0\text{--}4.5^\circ$) below the projection of the center of the optic disc (the results were comparable in the two species of flying fox). Finally, the position of the area centralis in the visual field was considered as the intersection between the VM and the HM. Although the distance between the optic disc and the VM could also be roughly estimated by the peak of ganglion cell density, we preferred to rely on the electrophysiological determination since it could be done for each case separately, thus eliminating the effects of interindividual variability and the possibility of different degrees of shrinkage during the histological processing of the retinas. Further-

more, there is evidence that the VM passes lateral to, rather than exactly through, the center of the peak of ganglion cells in nocturnal animals (Volchan et al., '88; Hokoç et al., '92), therefore introducing a further source of uncertainty in the calculations based on retinal flat-mounts.

RESULTS

We shall first summarize the topographic organization of V1 in relation to the gyral morphology of flying foxes, and then substantiate the existence of a detailed retinotopic map by showing receptive field sequences and flat reconstructions of V1. The electrophysiological and histological criteria for determination of the boundaries of V1 will be presented next. Finally, a quantitative analysis of the variation of cortical magnification factor and receptive field size in different portions of V1 will be presented.

Location and overall organization

The main features of the organization of V1 are similar in the two species of flying foxes we studied. As shown in Figure 2, the primary visual area (area 17, or V1) in *Pteropus* occupies the posteriormost portion of the occipital lobe. In each hemisphere, V1 contains a continuous and precisely ordered first-order representation of the complete contralateral hemifield. The representation of the area centralis is located anteriorly in the dorsal surface of the occipital lobe, and more peripheral portions of the visual field are represented along the tentorial and mesial surfaces and along the upper bank of the splenial sulcus. The representation of the HM runs across the dorsal and tentorial surfaces and the splenial sulcus, dividing V1 in such a way that the lower visual quadrant is represented medially and the upper quadrant laterally. The VM representation, together with a small ipsilateral field representation, forms the anterior border of V1 with visual extrastriate cortex. The remaining parts of the perimeter of V1, mostly in the splenial sulcus, are formed by the representation of the visual periphery. The projection of the visual field onto V1 is distorted, in the sense that it emphasizes the representation of the central visual field relative to that of the visual field periphery. The central retina is more magnified in *P. poliocephalus* than in *P. scapulatus*, and therefore a more restricted portion of the central visual field is represented in the dorsal surface in the former species.

Retinotopic organization of V1

Figure 3 illustrates the locations of receptive field centers in the visual field and the corresponding recording sites in V1 in a series of parasagittal sections of a *P. scapulatus* brain (case PS5). In each section plane, the sequence of receptive field centers moves from a central location, close to the anterior boundary of V1 on the dorsal surface of the brain (e.g., fields A1, C1, D1, E1, F1), into the visual field periphery, as successive sites along the tentorial surface and dorsal bank of the splenial sulcus are sampled. Only the central $30\text{--}35^\circ$ of the visual field are represented on the dorsal surface of the occipital lobe. The lateral portions of V1 represent the upper visual quadrant (planes A, B, and C), while the lower quadrant is represented medially (planes E, F, and G). The projection of the visual field onto V1 in the flying fox is retinotopically precise: the sequences of receptive fields recorded along the surface of the cortex are

Fig. 2. Summary view of the visual topography of V1 in the flying fox. **A, B:** Dorsocaudal views of the left hemisphere of a *P. poliocephalus* (A) and a *P. scapulatus* (B), tilted 30° from the vertical along the sagittal plane. **C–E:** Ventral, ventrocaudal (30° below the horizontal), and medial views of a *P. scapulatus* brain, respectively. In all parts, striate cortex is shown in white, as compared with the dark grey of other portions of the brain, and the excised brainstem (hatched areas). The VM is shown in filled squares, the HM in circles, the periphery of the visual field in filled triangles, the center of gaze in stars, isoazimuths in thin continuous lines, and isoelevations in thick dotted lines, as indicated by the central insert. In C and E, the ventral bank of the posterior part of the splenial sulcus was retracted in the direction indicated by the arrows in order to allow the visualization of the peripheral representation.

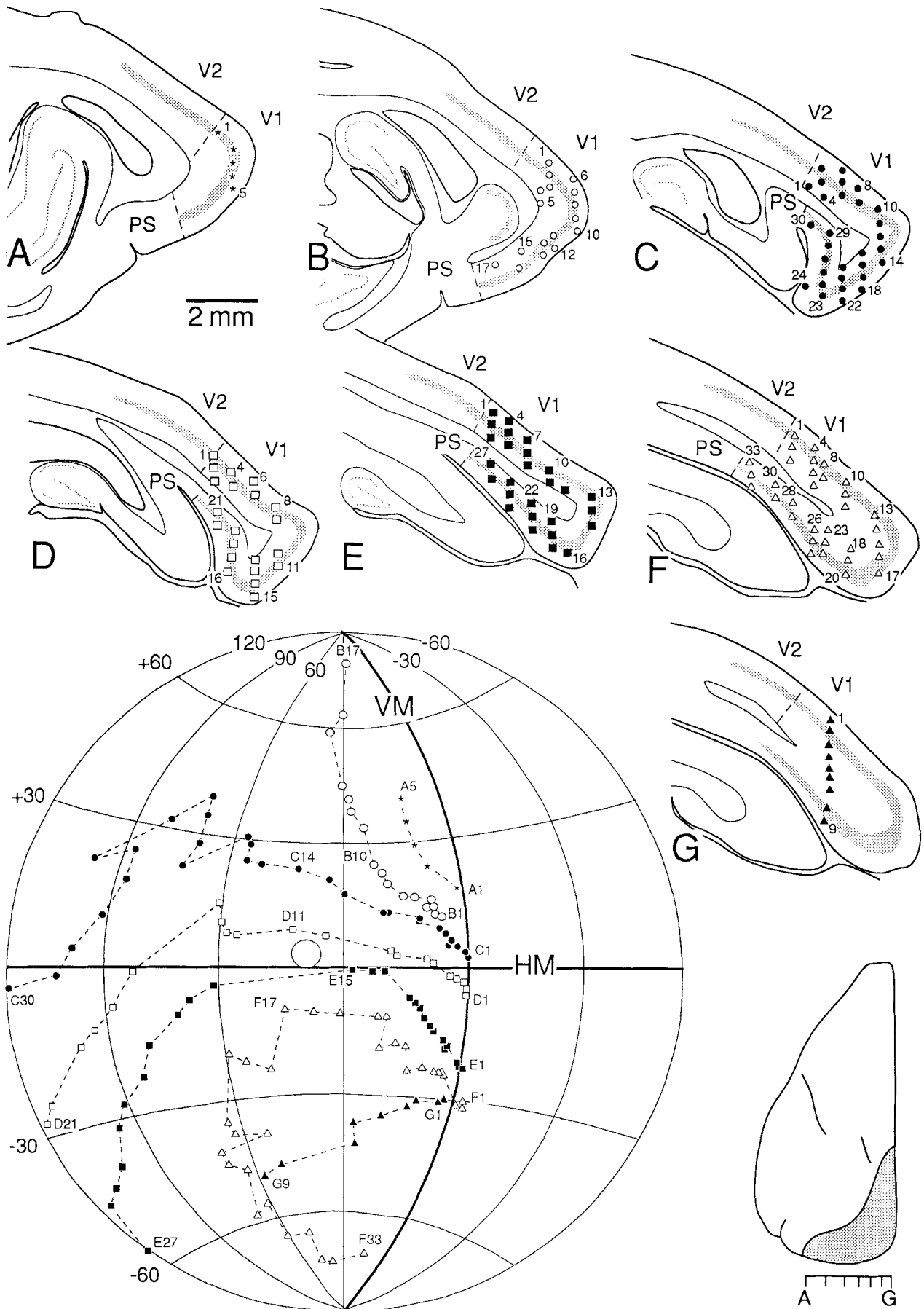


Figure 3

relatively smooth, and sequences corresponding to different mediolateral levels do not overlap.

In order to interpolate the representation of isoelevation and isoazimuth lines and to obtain a more detailed view of the retinotopic organization of V1, we projected the recording sites shown in Figure 3 onto a graphically "unfolded" representation of the occipital cortex. Figure 4A shows a two-dimensional map of the portion of the occipital cortex characterized by a cytochrome oxidase-rich layer IV. As shown below, this region includes V1 and at least another visual area. The map in Figure 4A shows the contours of layer IV in the sections used to generate the map and the recording sites, numbered as in Figure 3. In order to minimize the distortion involved in generating a bidimensional representation of the complex tridimensional form of V1, a discontinuity was introduced along the representation of the peripheral visual field. In Figure 4B, the retinotopic map of V1 was interpolated conforming to the position of the receptive field centers in the visual field. As shown in Figure 4, the recording sites in this case were distributed through most of V1, therefore allowing us to generate a nearly complete map of its visual topography. It is possible to observe, for example, that the HM representation bisects V1 so as to form nearly equal halves dedicated to the lower and upper quadrants. In addition, one can observe that the representation of the area centralis is far more magnified than that of the visual periphery: for example, compare the distance along the HM representation between the 0° and 10° isoazimuth lines with that between the 100° and 110° isoazimuths. Finally, the unfolded representation better illustrates the existence of a thin strip of cortex (approximately 0.7 mm wide) at the anterior portion of V1 that represents a portion of the ipsilateral hemifield. Based on receptive field sizes and architecture (see below), we consider this region to be a transitional zone between V1 and the extrastriate cortex. The surface areas of V1 in the specimens of *P. scapulatus* we studied were 107, 110, and 115 mm², after correction for shrinkage.

The visual topography of striate cortex in *P. poliocephalus* can be described as an enlarged version of the organization observed in *P. scapulatus*. The summary of data from a nearly completely mapped striate cortex of a *P. poliocephalus* (PP4) is shown in Figures 5 and 6. Note that, in spite of the larger surface area of V1, the location of the architectonic boundaries of V1 in relation to the gyral morphology is very similar in the two species of flying fox. The surface areas of V1 in three *P. poliocephalus* were 110, 130, and 182 mm².

Fig. 3. Retinotopic organization of V1 in a *P. scapulatus*. **Upper:** Parasagittal sections through the left hemisphere of the brain, from lateral (A) to medial (G). In each section, the region with a heavily cytox-stained layer IV is shown in grey, and the borders of V1 in dashed lines. The recording sites are shown with different symbols for each parasagittal level and are numbered sequentially according to their radial projection to layer IV. V1 is the primary visual area, V2 the second visual area, and PS the prostriate area. **Lower left:** Location of receptive field centers corresponding to the sites shown in sections A–G. The field centers are shown in an equatorial-zenithal chart, according to the symbols used in the respective sections. The VM and HM are shown by thick lines, and the projection of the optic disc by the white circle. The VM was rotated in the chart in order to illustrate the azimuths up to 120°. **Lower right:** Insert showing the level of sections A–G in relation to V1 (grey area), in a dorsocaudal view of the left hemisphere.

The total extent of the visual field represented in V1 coincides with the field of vision of the flying fox (Fig. 7). The field of vision was inferred for each case by plotting the point at which the corneal reflex of a punctiform light source observed along the optic axis of the eye disappears (Sousa et al., '78a). Based on this method, the average monocular field of vision along the HM extends to approximately 125° temporal and 60° nasal to the VM. The boundary between the binocular and the monocular sectors of V1 is approximately coincident with the upper lip of the splenial sulcus.

Electrophysiological determination of the borders of V1

Abrupt changes in the progression of receptive field centers, as well as in receptive field sizes, were the criteria used to define the borders of V1. These criteria, which allow the functional determination of the striate/prestriate border during the ongoing recording session, are illustrated in Figure 8. Figure 8A shows the dorsal aspect of striate cortex in *P. poliocephalus* PP3, as viewed through a craniotomy extending from the midline to the vicinity of the lateral edge of striate cortex, exposing the representation of the central 20–30°. The typical pattern of blood vessels in the occipital cortical surface of *Pteropus*, running from posteromedial to anterolateral, is also illustrated. The recording sites, all from a depth of 800 μm, are shown organized in parasagittal rows. In each row, the centers of the receptive fields recorded at sites progressively closer to the anterior border of V1 (Fig. 8C, dots) approach the VM, and receptive field centers actually invade the ipsilateral hemifield by a few degrees (see, for example, row 31–38). The sequence then reverses, and the receptive fields re-represent the central portion of the contralateral hemifield, now in a prestriate area (Fig. 8C, squares). The point of reversal is coincident with a sudden increase in receptive field size (Fig. 8D). In all cases, the receptive fields recorded in the area anterior to V1 on the dorsal surface seemed to form a single, approximately mirror-symmetrical representation in relation to that found in V1, and this area is here referred to as V2 (Thompson et al., '50; Allman and Kaas, '74; Albus and Beckmann, '80; Gattass et al., '81; Rosa et al., '88b).

The extent of the region of overlap between the visual representations in the two cerebral hemispheres (Clarke and Whitteridge, '76) was specifically explored in one animal (PP1) with a fine grid of penetrations along the V1/V2 border on the dorsal surface of both hemispheres. Figure 7 summarizes the extent of the ipsilateral representation in the border region, based on pooled data from this and all the other animals. If one considers the borders of the receptive fields, the ipsilateral invasion does not exceed 8° along the HM, but may reach as much as 14° at eccentricities of 30° or more. This is a minimum estimate, since, due to the relative inaccessibility of the border between V1 and V2 at the peripheral VM representation, this region was not as well studied as the central representation. Hence a larger invasion may occur in the periphery.

The border of V1 in the splenial sulcus corresponds to the representation of the temporal edge of the field of vision (Figs. 3–6). Although several recording sites were sampled in the area immediately anterior to the peripheral representation, no visual drive was obtained under our recording conditions. This area is characterized by a very rich spontaneous activity, commonly consisting of neuronal spikes of large amplitude, and these characteristics correspond to

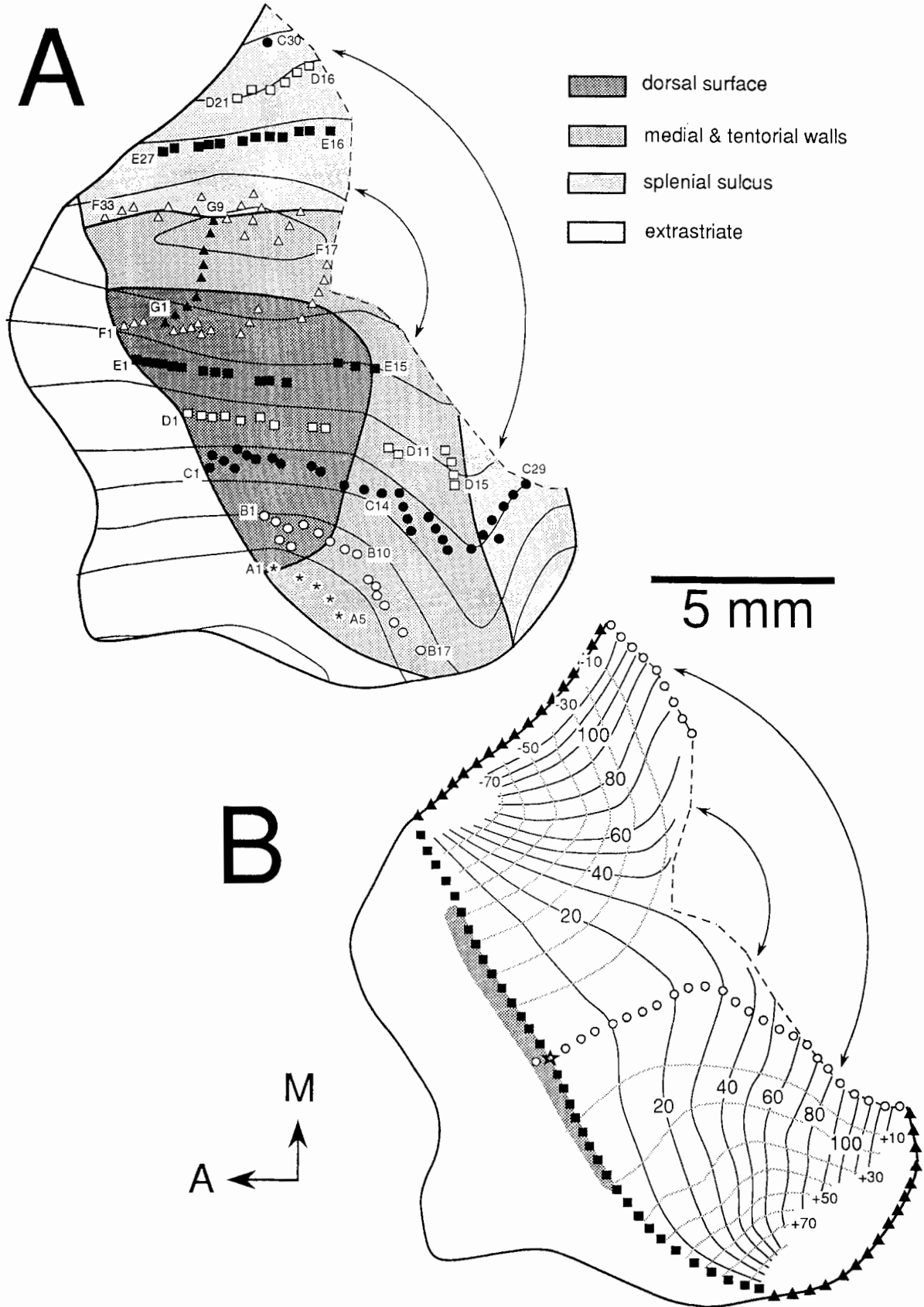


Figure 4

those of the area prostriata as defined in the anesthetized monkey (Gattass et al., '87).

Histological determination of the boundaries of V1

Figure 9 shows the histological correlates of the physiological transitions we observed at the boundaries of V1. These boundaries are identifiable by low-power (10–20 \times) examination of sections stained for cytox, Nissl, and myelin.

In cytox-stained sections (Fig. 9A), the anterior boundary of V1 with V2 is characterized by a change in the appearance of the cytox-rich layer IV. While in V1 this layer is thicker and has sharply defined limits, in V2 it is thin and fuzzy. The boundary of V1 in the splenial sulcus, on the other hand, is sharp and clearly defined, since the area prostriata stains lightly for cytox in all cortical layers (Fig. 9A).

With myelin stains, area V1 appears in parasagittal sections as a heavily myelinated region, with a dark and homogeneous outer band of Baillarger. This band is thicker in the central representation, and thins out towards the peripheral representation (Fig. 9B). Prestriate area V2 is less myelinated than V1, and presents heterogeneities in the density of myelination (Fig. 9B). The boundary between striate and prestriate cortex is better appreciated, however, in flat-mounted preparations (Fig. 9C). In these cases, the limit between V1 and V2 appears more sharply defined than in conventional sections. Area prostriata, as in other mammals (Sanides and Hoffman, '69; Tusa et al., '78; Gattass et al., '87) stains lightly for myelin, and is readily separable from V1 (Fig. 9B).

In Nissl-stained sections, the V1/prostriata border is likewise sharply defined, by the near absence of a granular layer IV in the latter (not illustrated). The anterior border of V1 with V2, on the other hand, is more difficult to define precisely. However, the determination of the limits of V1 and V2 is possible, based on the characteristics of layer IV, which is thicker in V1 than in V2.

Cortical magnification factor

The cortical magnification factor (CMF), i.e., the ratio between the distance between two points in the cortex and the corresponding angular distance between receptive field centers in the visual field, was studied in two animals. The data from a *P. poliocephalus* (Fig. 10A) and from a *P. scapulatus* (Fig. 10B) are illustrated as a function of eccentricity. In both cases, the variation of CMF with eccentricity can be approximated by a power function. The peak CMF in the representation of the central retina is higher in *P. poliocephalus* than in *P. scapulatus*, but the values in the peripheral representation are similar. Therefore, the larger surface area of V1 in the former is largely

due to an expansion of the central representation, rather than a uniform re-scaling. We also tested the data for a systematic variation of CMF with polar angle. The data corresponding to different isopolar sectors in the visual field are shown with different symbols in Figure 10. No statistical difference was observed between functions fitted separately to the data along the HM, the VM, and the 45 $^\circ$ isopolar lines.

Some irregularities in the CMF that were consistently observed in both *P. poliocephalus* and *P. scapulatus* are best appreciated by referring to the flat reconstructions shown in Figures 4 and 6. Particularly along the peripheral HM representation, the CMF is larger along the isoazimuth lines (i.e., along the direction parallel to the V1/V2 border) than along the isoelevation lines. In Figure 10, the anisotropic representation is reflected by the larger scatter in the CMF data along the HM in comparison with other meridians. Note that, in regions representing the upper and lower peripheries of the visual field, the larger distance between isoelevation lines, as compared with isoazimuth lines, reflects the convergence of the meridians in the poles of the equatorial-zenithal system, and does not indicate an anisotropy in the representation.

Receptive field size and point-image size

The variation of the receptive field size in V1 (calculated as the mean of the four sides of the rectangular receptive fields) with eccentricity is shown in Figure 11. For both *P. poliocephalus* and *P. scapulatus*, the variation can be approximately described by a linear function with an angular coefficient close to 8% of the eccentricity value. The difference in the value of the y-intercepts observed between the two illustrated cases mostly reflects the better fit to central data in case PP4 than in PS5, rather than systematically larger receptive fields in *P. poliocephalus*. No systematic differences were observed between receptive fields located along different isopolar lines (different symbols in Fig. 11).

An estimate of the linear dimension of the cortical region activated by a punctiform light source, i.e., the cortical point-image size (McIlwain, '76), was obtained by multiplying the CMF by the receptive field size at several eccentricities. Figure 12 shows our estimates of the point-image size for two animals (PP4 and PS5).

DISCUSSION

The main features of the retinotopic organization of V1 in *Pteropus* conform to the general mammalian plan: a continuous representation of the visual field, with lower quadrants represented dorsomedially, the upper quadrants ventrolaterally, central vision and the VM anteriorly, and the periphery of the visual field posteriorly (marsupials: Sousa et al., '78b; insectivores: Kaas et al., '70; rodents: Hall et al., '71; Drager, '75; Choudhury, '78; Wagor et al., '80; Picanço-Diniz et al., '91; lagomorphs: Hughes, '71; artiodactyls: Clarke and Whitteridge, '76; carnivores: Tusa et al., '78; McConnell and Le Vay, '86; Law et al., '88; tree shrews: Kaas et al., '72; primates: Daniel and Whitteridge, '61; Allman and Kaas, '71b; Gattass et al., '81, '87; Van Essen et al., '84). Accommodated within this basic plan, however, are variations that may reflect different specializations in the species' visual habits. In the following sections, we discuss the organization of V1 in the flying fox, with

Fig. 4. Flat reconstructions and summary maps of V1 in *P. scapulatus*. **A:** Flat reconstruction of the portion of the occipital lobe characterized by a cytochrome oxidase-rich layer IV. Different parts of V1 and the extrastriate area are shown in different tones of grey, as indicated in the key. The contours of layer IV used to generate the map are shown by the thin lines, and a discontinuity along the peripheral representation of V1 by dashed lines and arrows. Anterior is to the left, and medial is upwards (see key at lower left). Recording sites are indicated as in Figure 3. **B:** Interpolated map of the visual field representation in V1. Symbols as in Figure 2, with the exception of the region of ipsilateral representation at the anterior border of V1, which is shown in dark grey.

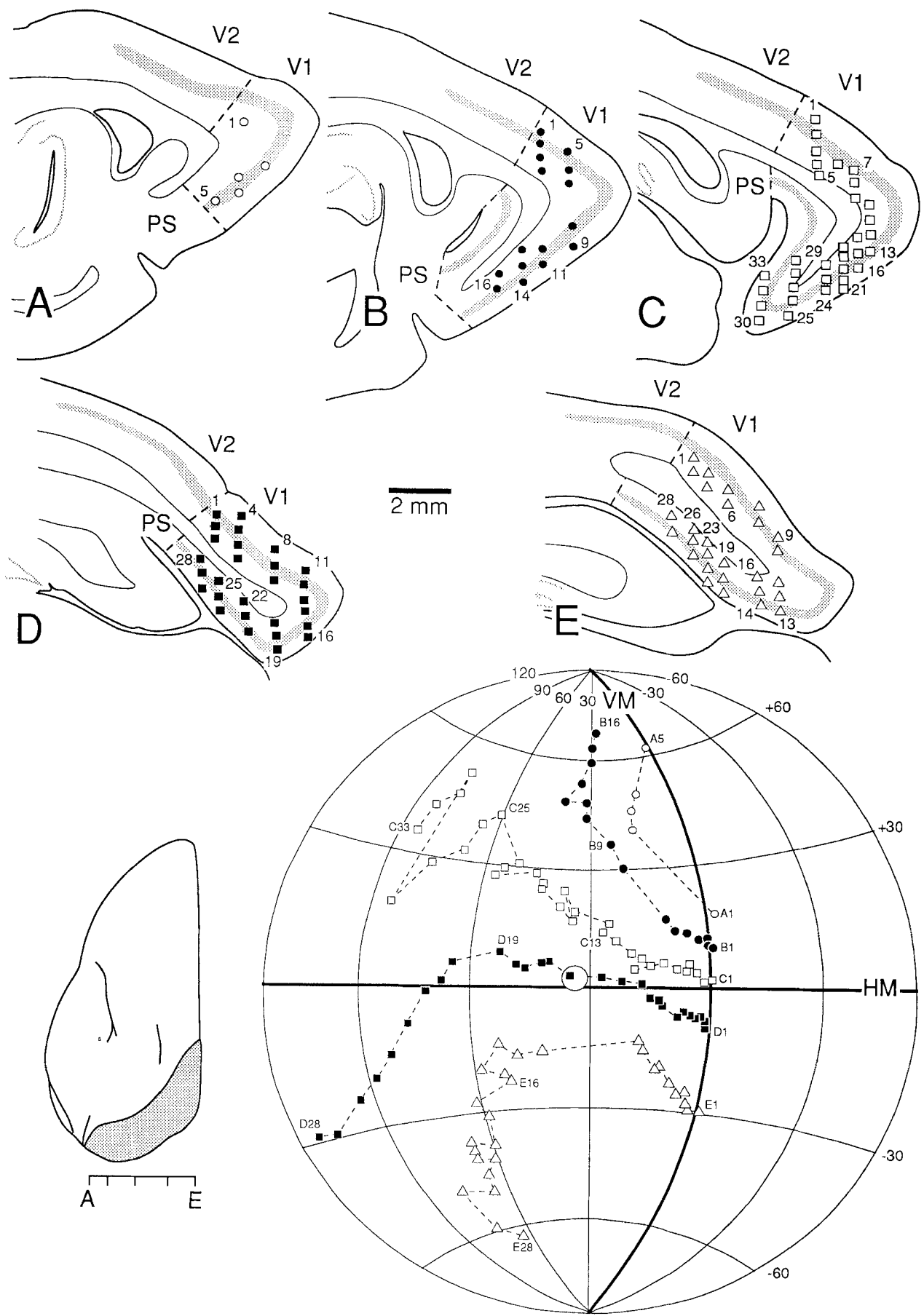


Figure 5

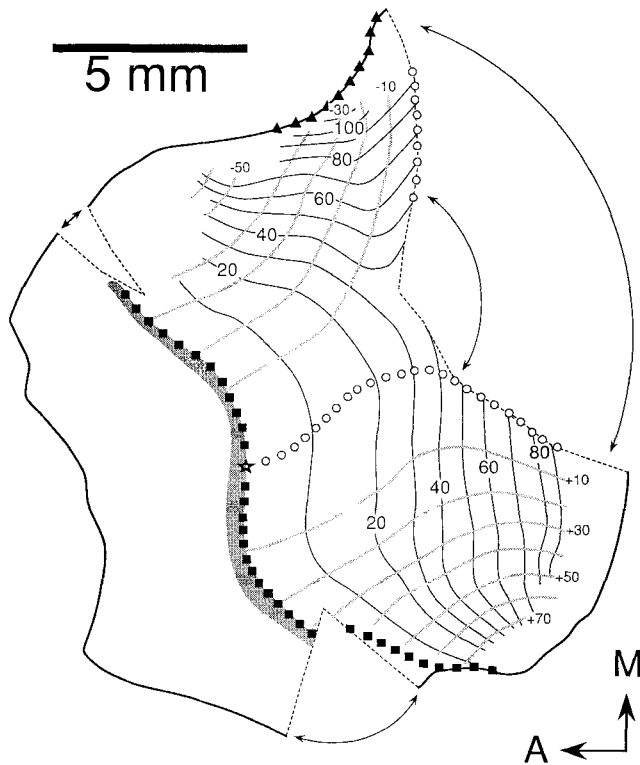


Fig. 6. Summary map of the retinotopic organization of V1 in a *P. poliocephalus*. Same case as shown in Figure 5. Conventions as in Figures 2 and 4B.

special emphasis on the comparison with members of other mammalian orders.

Surface area of V1 and allometric comparisons

In several respects, the organization of striate cortex in flying foxes reflects their reliance on the well-developed vision as the main means of telereception. Most notably, the surface area of striate cortex is large in relation to their body weight. An analysis of Figure 13 demonstrates, firstly, that there is a positive correlation between body weight and surface area of V1 among mammals in general, and, secondly, that the area of V1 in primates, whether nocturnal or diurnal, tends to be disproportionately large in comparison with similar-sized non-primates. In this context, the surface area of V1 in *P. poliocephalus* and *P. scapulatus* is larger than expected for a non-primate, but slightly smaller than that predicted for a nocturnal primate. For example, in the ferret, a nocturnal carnivore of similar body weight, the area of V1 ranges from 65 to 87 mm² (Law et al., '88), in comparison with 110–180 mm² in *P. poliocephalus* and 107 to 308 mm² in the slightly larger owl monkey (Krubitzer, '89). Our estimates of the surface area of V1 are based on planimetric measurements of graphically "unfolded" representations, a technique that may result in errors of up to 20–30% (Van Essen and Maunsell, '80). However, our reconstructions are considerably more accurate than this.

Fig. 5. Retinotopic organization of V1 in a *P. poliocephalus*. Same conventions as in Figure 3.

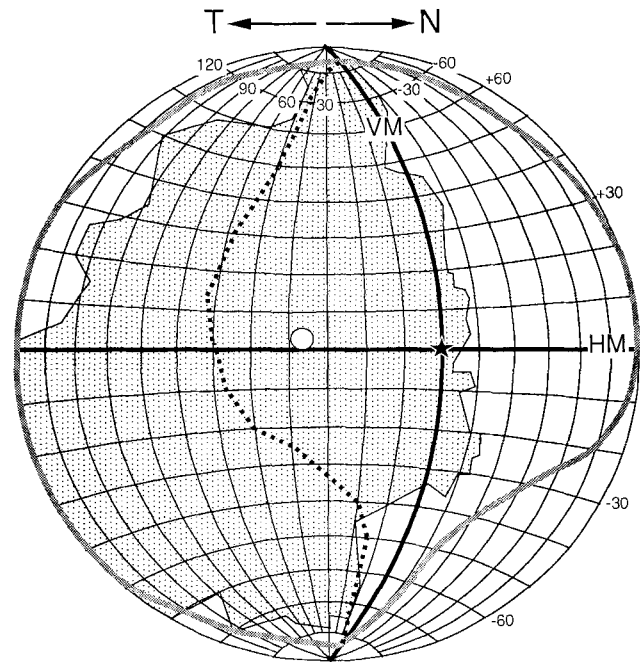


Fig. 7. The extent of the average unocular field of vision of four *Pteropus* spp. (thick grey line) is compared with the region of the visual field encompassed by all receptive fields recorded in this study (dotted fill). Receptive fields recorded in the right hemisphere were reversed along the VM, so all receptive fields are shown as if they were recorded in a left hemisphere. The VM and HM are shown by the thick black line, the optic disc by the white circle, the center of gaze by the star, and the temporal border of the binocular field of vision by the heavy dotted line. The temporal edge of the field of vision actually extended to 125° azimuth between the HM and the -40° elevation. T, temporal; N, nasal.

Due to the presence of fewer sulci and to the smaller area, the reconstruction of V1 in the flying fox is much simpler than the reconstruction of the whole neocortex of the monkey, the situation in which these margins of error were obtained. In addition, the use of reference needles to align the sections, the calculation of the correct distance between points in adjacent sections at short intervals, and the introduction of discontinuities ensure the preservation of isometry. Our estimates of the surface area of V1 also compare well with measurements obtained from physically flat-mounted striate cortices of two additional *P. poliocephalus* (101 mm², uncorrected for shrinkage) from the study of Krubitzer et al. ('93).

Extent of the monocular and binocular fields of vision

A second point of interest is the presence of an extensive region of binocular overlap that, along the HM, would be comparable to that observed in cats (Hughes, '76) and monkeys (Gattass et al., '87). In addition, the binocular field in *Pteropus* is asymmetric, with a larger extent in the upper quadrant. Nonetheless, extreme specializations for emphasis in the upper or lower quadrant that exist in many other mammals such as rats, rabbits, and horses (Hughes, '77) were not observed in the flying fox. The existence of frontal vs. laterally placed eyes in mammals is loosely correlated with the animal's ecological niche. As reviewed by Hughes (1977), there are several theories that try to explain the occurrence of frontalized vs. lateralized eyes

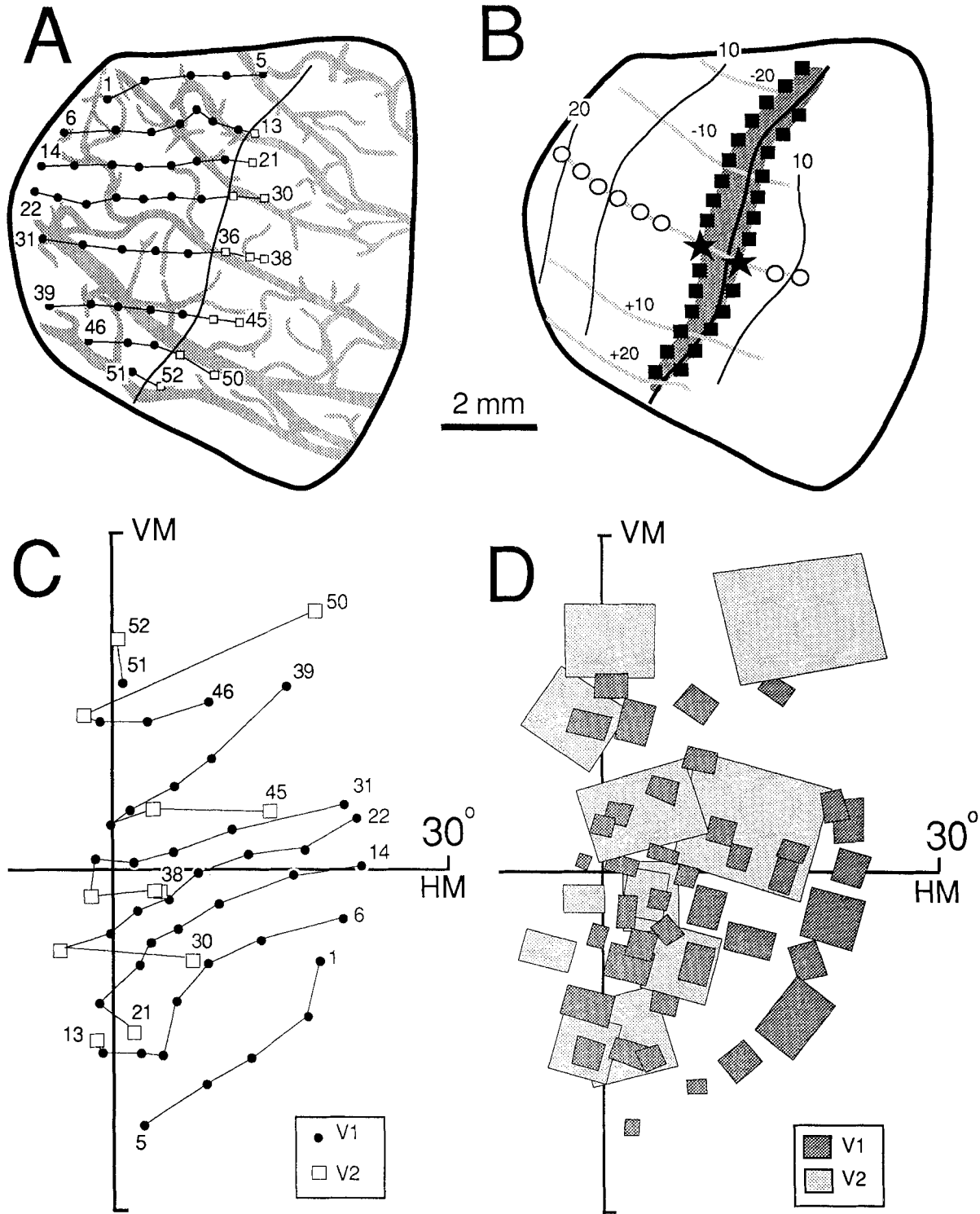


Fig. 8. Electrophysiological determination of the boundary of V1. **A** is based on a photograph of the striate/prestriate region in a *P. poliocephalus*, as viewed through a craniotomy (delimited by the thick line). Blood vessels are shown in grey, and the recording sites in V1 and V2 are shown by dots and squares, respectively. **B** is the interpolated

representation of the visual field in this region, based on the data shown in C and D. Conventions as in Figures 2 and 4B. **C** and **D** represent the central 30° of the visual field, with the receptive field centers (C) and borders (D) indicated. Note the reversal in the representation at the V1/V2 border (C) and the larger size of V2 receptive fields (D).

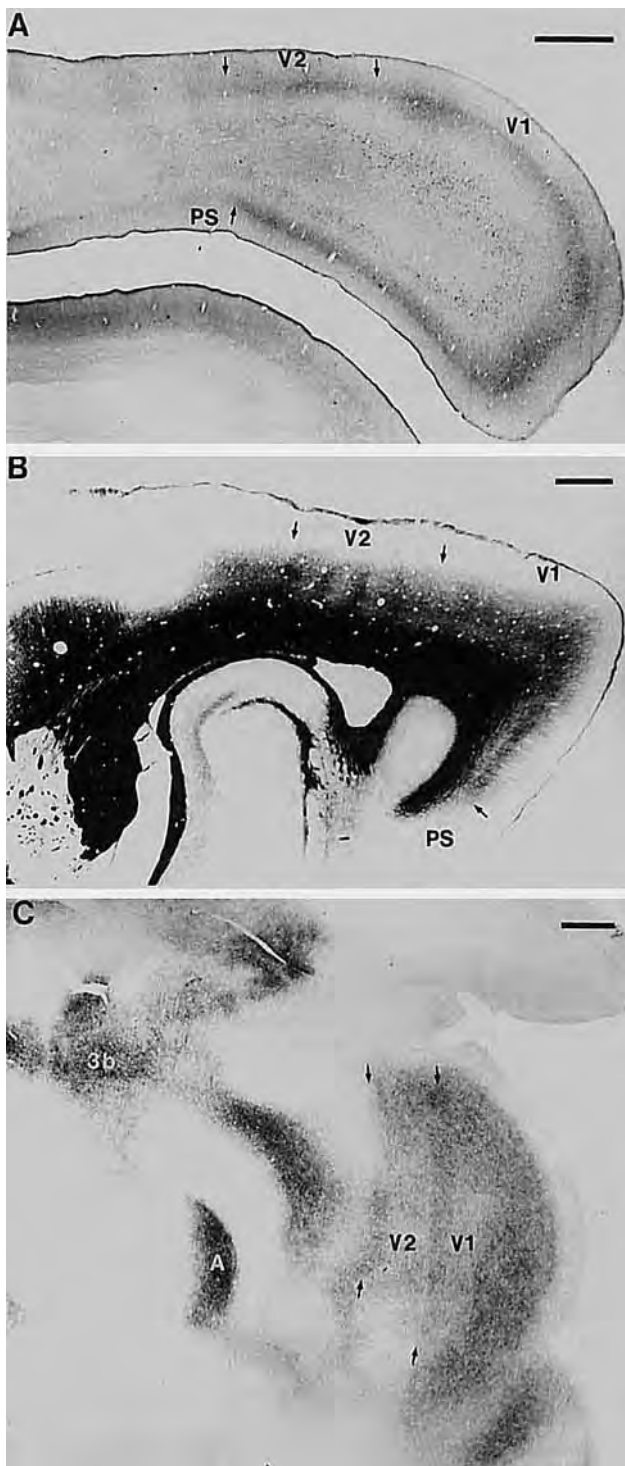


Fig. 9. Histological determination of the boundaries of V1. **A:** Cytochrome oxidase stain. This parasagittal section is close to the midline, and it is tangential to a portion of the cell-rich layer VI. **B:** Gallyas' myelin stain, parasagittal section. **C:** Gallyas' stain, section tangential to the cortical layers of a flat-mounted cortex. The location of somatosensory area 3b and of the primary auditory cortex (A) are also indicated. In all panels, arrows point to the areal boundaries, and the scale bars = 1 mm (uncorrected for shrinkage).

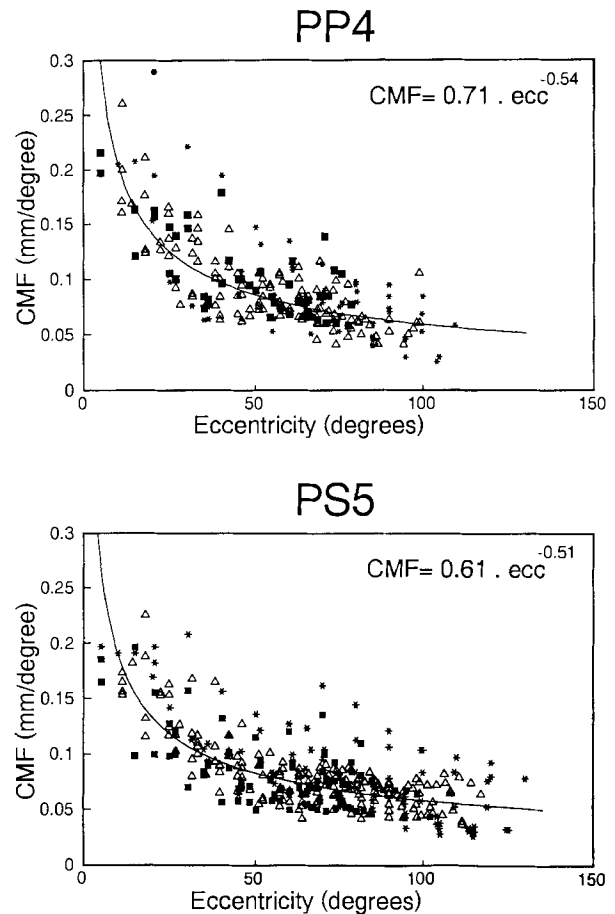


Fig. 10. Cortical magnification factor as a function of eccentricity in a *P. poliocephalus* (**upper**) and a *P. scapulatus* (**lower**). Different symbols correspond to pairs of receptive fields with average coordinates in different polar sectors: filled squares correspond to pairs in a range of polar angles within 22.5° of the VM, asterisks within 22.5° of the HM, and triangles within 22.5° of the 45° isopolar lines. The thin line represents the best-fitting power function, given in the upper right corner of the boxes. CMF, cortical magnification factor; ecc, eccentricity.

among mammals based on behavioral considerations, but none is entirely satisfactory. For example, it is generally true that a wide region of binocular overlap is present in predators, which may use binocular disparity clues to achieve a better localization of the prey and more efficiently direct the attack (Sousa et al., '78a); in contrast, animals that are preyed upon tend to have more laterally placed eyes. The flying fox, a fruit-eating bat, seems to violate the rule. Likewise, the extent of the field of vision of the flying fox is incompatible with theories based on a correlation between a wide binocular field and the manipulative ability of the species (see Hughes, '77 for a review). In *Pteropus*, due to the obvious specialization of the forelimb, most or all of the manipulation of the environment is dependent on the mouth; nonetheless, a wide binocular field is available. In this animal, the large binocular overlap may be a consequence of the optical constraints to the formation of focused images in large-aperture eyes such as those of the flying fox. The eyes of *Pteropus*, like those of many other nocturnal animals with developed vision (e.g., owls), have very low "f" ratios, and therefore limitations such as a small depth of

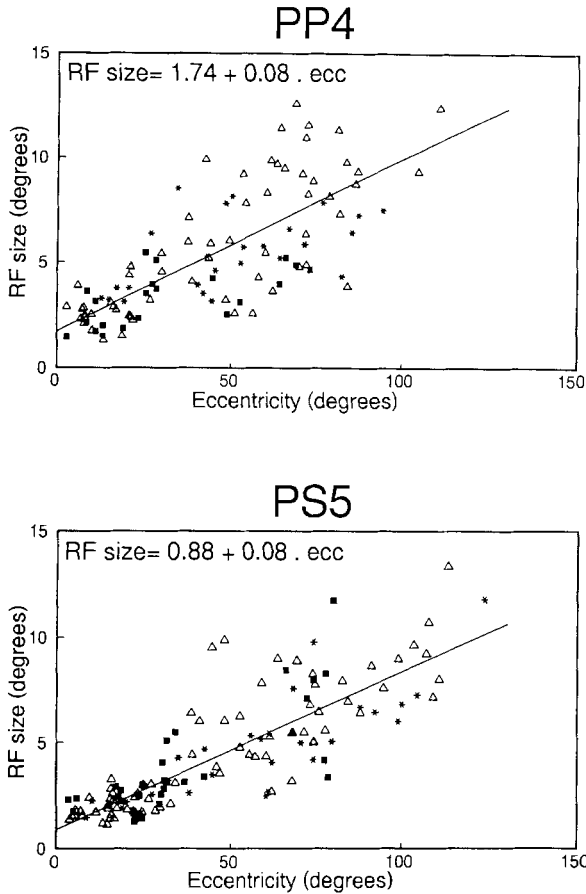


Fig. 11. Receptive field size as a function of eccentricity in a *P. poliocephalus* (upper) and a *P. scapulatus* (lower). Different symbols correspond to receptive fields with centers in different polar sectors, as in Figure 10. The thin line represents the best-fitting linear function, given at the top of each box. RF, receptive field.

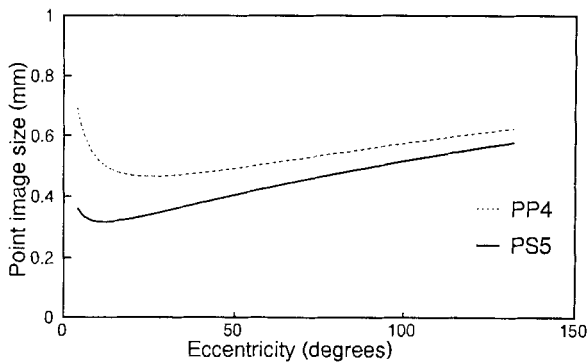


Fig. 12. Cortical point-image size as a function of eccentricity in two animals. For details, see text.

field and a high degree of optical aberration for off-axis light rays apply. As proposed by one of us (Pettigrew, '79), the latter property may impose a selective pressure to bring the area centralis closer to the optic axis, therefore resulting in frontalized eyes. As an indirect evidence on this subject, in

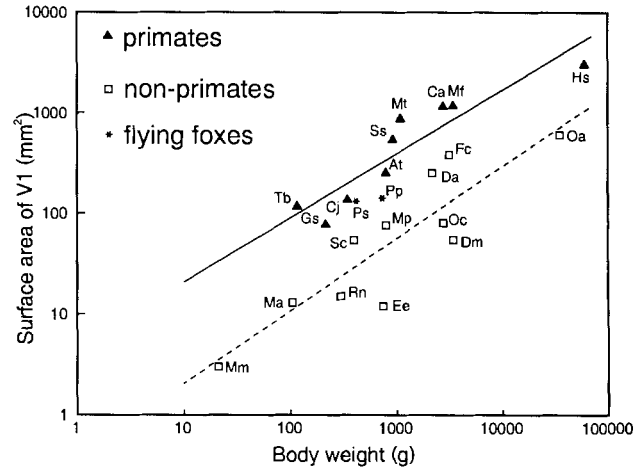


Fig. 13. Correlation between body weight and surface area of V1 in mammals. Each data point is identified by the initials of the name of the species. Separate power functions were fitted to the data obtained from primates (solid line) and non-primates (dashed line). The best-fitting functions were $V1\ surface\ (mm^2) = 0.39 \cdot body\ weight\ (g)^{0.72}$ ($R^2 = 0.78$) for non-primates, and $4.8 \cdot body\ weight^{0.64}$ ($R^2 = 0.82$) for primates. The sources of data on dimensions of V1 and abbreviations are At, owl monkey (average of values given by Tootell et al., '85; Krubitzer, '89); Ca, capuchin monkey (average of values in Gattass et al., '87; Rosa et al., '88a, '91, '92a); Cj, marmoset (Krubitzer, '89); Da, agouti (measurement of the flat reconstruction illustrated by Picanço-Diniz et al., '91); Dm, South American opossum (Sousa et al., '78b); Ee, hedgehog (calculation based on data illustrated by Kaas et al., '70); Fc, cat (Tusa et al., '78); Gs, bushbaby (Krubitzer, '89); Hs, human (measurements from flat-mounted human V1, unpublished observations); Ma, hamster (Sousa et al., '78b); Mf, Java macaque (Van Essen et al., '84; Florence and Kaas, '92); Mm, mouse (Drager, '75; Sousa et al., '78b; Wagor et al., '80); Mp, ferret (Law et al., '88); Mt, talapoin monkey (Florence and Kaas, '92); Oa, sheep (calculation based on values given by Clarke and Whitteridge, '76); Oc, rabbit (Hughes, '71; Sousa et al., '78b); Rn, rat (Montero et al., '73; Sousa et al., '78b); Sc, squirrel (measurement of flat-mounts illustrated by Kaas et al., '89); Ss, squirrel monkey (Krubitzer, '89); Tb, tarsier (measurement of a graphic reconstruction of Nissl-stained striate cortex; M.G.P. Rosa and J.D. Pettigrew, in preparation). Unless the body weight of the experimental subjects is given by the authors of each paper, body weights represent the average for the species (Nowak and Paradiso, '83).

Rousettus, another member of Pteropodidae, but adapted to a cave environment and to the use of echolocation, the extent of the binocular field seems to be much more restricted (Thiele et al., '91), possibly due to a much lesser selective pressure for the formation of high-quality images. In addition, the absolute sensitivity threshold and visual acuity are increased under binocular, as compared with monocular viewing conditions (Hughes, 1977). Therefore, the ability to sample a large region of the visual field with two eyes simultaneously may be of special functional advantage for a nocturnal animal that is as dependent on vision for normal behavior as a flying fox.

Radial symmetry in the representation and anisotropy

In the flying fox, the representation of the upper and lower quadrants is approximately symmetrical, in terms of magnification factors. In some animals (e.g., Fig. 4), the central representation of the upper quadrant appears to be

more magnified than that of the lower quadrant, but this may only reflect small errors in the calculation of the position of the area centralis. In any event, these differences would be small compared with those observed in ground-dwelling species such as the rabbit (Thompson et al., '50; Hughes, '71), cat (Tusa et al., '78), ferret (Law et al., '88), and agouti (Picanço-Diniz et al., '91). While adopting the normal, upright posture during flight, flying foxes rest and feed mostly by hanging upside down from tree branches. We might speculate, therefore, that the symmetry in the visual representation of upper and lower quadrants reflects the fact that, in the flying fox, these quadrants are less specialized for different patterns of stimulation than in ground mammals. Interestingly, among primates, asymmetries in the representation of upper and lower quadrants were observed in macaques (Van Essen et al., '84, '90; Maunsell and Van Essen, '87), but are not marked in the more arboreal owl monkey and *Cebus* monkey (Allman and Kaas, '71a,b, '74; Gattass et al., '87; Rosa et al., '88b; Fiorani et al., '89).

We also observed an anisotropy in the representation of the visual field, in the sense that an equal distance in the visual field is represented by a larger distance in the cortex along the isoazimuth lines than along the isoelevation lines. This observation is valid, however, only for the representation of the portions of the visual field along the HM, and away from the area centralis. In other mammals such as the cat (Tusa et al., '78; Albus and Beckmann, '80), the hamster (Tiao and Blakemore, '78), and especially the rabbit (Hughes, '71), this anisotropy seems to be more marked, and to be present throughout the visual field representation. In primates, anisotropies in the representation of the visual field periphery in V1 (Tootell et al., '88; Gattass et al., '90) and throughout V2 (Rosa et al., '88b) were shown to be correlated to the pattern of ocular dominance and cytochrome oxidase stripes, respectively, so that the magnification factor would be larger perpendicular to the stripes. So far there is no evidence of ocular dominance stripes or functionally different modules in the flying fox striate cortex, but the above observations suggest that, if present, these columns or modules may not form a systematically oriented pattern for most of V1.

Invasion of the ipsilateral hemifield

The existence of a strip of ipsilateral representation at the anterior boundary of V1 in various mammals is now well documented (Kaas et al., '70; Hall et al., '71; Drager, '75; Clarke and Whitteridge, '76; Tiao and Blakemore, '78; Kennedy et al., '85; Volchan et al., '88; Payne, '90). In the flying fox, the extent of this ipsilateral invasion along the HM (8°) is larger than that observed in cats (4°, Payne, '90). However, the width of the overlap zone in cats and flying foxes is similar in the mid-peripheral representation. Comparisons with other species are limited by the fact that recordings at several elevations in the visual field are not generally documented. Taking into consideration the representation of the HM, one would conclude that the total extent of the invasion (based on receptive field borders) in the flying fox is larger than that in the baboon (Kennedy et al., '85), but smaller than that in sheep (Clarke and Whitteridge, '76) and opossums (Volchan et al., '88). Based on the abrupt change in receptive field size, we were able to determine that the V1/V2 boundary corresponds to the representation of the ipsilateral hemifield close to the VM,

rather than at the representation of the VM itself. A similar conclusion was reached by Kennedy et al. ('85), based on changes in receptive field properties along the baboon's V1/V2 boundary.

Comparison between retinal and cortical topography

As shown in Figure 10, the linear magnification factor in the flying fox's cortex decreases by a factor of 4–6 times from the central to the peripheral retina. Therefore, in areal terms, the central representation is approximately 25 times as magnified as the far periphery. This is in contrast with the gradient of retinal ganglion cell densities, which changes only by a factor of 8 (Pettigrew, '86; Graydon et al., '87; Dann and Buhl, '90). It is presently unclear whether this "over-representation" of the central retina in the cortex is a general mammalian feature or a specialization present in some groups only. In one of the best-documented species, the cat (Tusa et al., '78), and also possibly the ferret (Law et al., '88), the ganglion cell density in the retina and the CMF in V1 seem to vary in parallel, as predicted by the hypothesis of scaling of the central representations by the density of sampling channels in the periphery (Woolsey et al., '42). Although the issue of "peripheral scaling" of the cortical representation in primates is still the subject of debate (Schein and de Monasterio, '87; Wassle et al., '89), in several species of both nocturnal and diurnal monkeys there is a much larger representation of the central visual field in the cortex than that expected based on ganglion cell counts in Nissl-stained flat-mounted retinas (Myerson et al., '77; Perry and Cowey, '85; Silveira et al., '89). The discrepancy between retinal and cortical topography was also reported in the representation of the HM in V1 of rabbits (Hughes, '71) and rodents (Picanço-Diniz et al., '91). In addition, we observed no difference between the CMF measured in different polar sectors, in spite of the presence of a radial asymmetry in the distribution of ganglion cells in the retina (Fig. 1B).

Multi-unit receptive field sizes in the striate cortex of *Pteropus* are comparable in size to those obtained in cats under identical conditions (M.G.P. Rosa and L.M. Schmid, manuscript in preparation). In linear terms, the size of receptive fields in the flying fox's central V1 is about one-fifth of that in peripheral V1. This gradient is much steeper than that expected based on the retinal topography of *P. scapulatus*. In this species, the diameter of the dendritic fields of both alpha and beta-type ganglion cells changes only by a factor of approximately 2 along a similar range of eccentricities (Dann and Buhl, '90). Once again, the data point to a larger degree of convergence in the peripheral representations than in the central representations along the retino-geniculo-cortical pathway. In rodents, it has been suggested that the mismatch between the retinal and cortical topography may reflect the existence of specialized peaks in ganglion cell density related to the different classes of ganglion cells (Picanço-Diniz et al., '91). In the flying fox, the mismatch between V1 receptive field sizes and the diameters of dendritic fields of retinal ganglion cells is similar regardless of the class of ganglion cell used for comparison.

Point-image size

The cortical point-image size represents the diameter of the cortical region in which the receptive fields contain the

representation of a given point of space. Therefore, all the neuronal machinery necessary to analyze the visual field location in consideration must be contained in this estimate. In our study, the cortical point-image size in V1 was estimated by the product of the receptive field size and cortical magnification factor. This method is obviously limited, since it does not consider the scatter in receptive field position that is usually observed in radial penetrations across the cortical layers (Hubel and Wiesel, '74), and therefore the estimates are more appropriately referred to as "minimum point-image size" (Rosa et al., '88b). Nonetheless, previous experience shows that, in spite of the lower absolute values, the curves of minimum point-image size accurately reflect the changes in the total point-image size (Fiorani et al., '89). In both species of flying fox (Fig. 12), there is little, if any, change in the value of the point-image size as one moves from the central to the peripheral representation. The apparent changes (e.g., the minima at the central representation) are within the limits of precision of the fitting of linear and power functions used in the calculation, and it is perhaps more appropriate to say that the minimum point-image size in both species of flying fox is close to 0.5 mm throughout V1. In comparison, in several areas of the primate (Dow et al., '81; Van Essen et al., '84; Maguire and Baizer, '84; Gattass et al., '87, '90; Rosa et al., '88b), feline (Albus, '75), and rodent (Picanço-Diniz, '87) visual cortex, point-image size varies markedly with eccentricity (but see Fiorani et al., '89, for a counter-example). The near constancy of the point-image size in the flying fox striate cortex is reminiscent of the concept of nearly invariant, modular "blocks" of cortex that would perform a similar series of logical operations on inputs arising from each part of the visual field, as originally proposed by Hubel and Wiesel ('74).

CONCLUSIONS

We have described the location, visuotopic organization, and histological correlates of the primary visual area in two closely related species of megachiropterans. To our knowledge, this is the first detailed report on the visual cortex of any bat. The general conclusion is that the primary visual area in *Pteropus* is surprisingly developed. However, it also seems to lack the specializations that are observed in other mammalian groups, as extreme asymmetries and anisotropies in the representation. In the context of the hypothesis that megachiropterans are a close sister group of primates (Pettigrew, '91) perhaps the most relevant piece of evidence comes from the allometric relationships between the size of V1 and body weight. This analysis establishes a difference between primates and non-primates, and sets *Pteropus* apart from other non-primate mammals. We believe that our quantitative study of the primary visual area in the flying fox will establish a useful basis for comparisons with other mammals of contrasting life styles, and with future studies of other visual structures.

ACKNOWLEDGMENTS

The authors acknowledge the support received from Dr. Michael Calford in several phases of this work, as well as Dr. Carlos Eduardo Rocha-Miranda and Ms. Rowan Tweedale, who gave several suggestions that improved the manuscript. We thank Katrina Schmid for taking the measure-

ments of the corneal curvature of flying foxes, Rita Collins and Guy Elston for help with the histology and preparation of the figures, and Michael Ward for the design and construction of the stereotaxic apparatus and accessories. Pavulon was generously donated by Organon (Australia) Pty. Ltd.

LITERATURE CITED

- Albus, K. (1975) A quantitative study of the projection area of the central and the paracentral visual field in area 17 of the cat. I. The precision of the topography. *Exp. Brain Res.* 24:159-179.
- Albus, K., and R. Beckman (1980) Second and third visual areas of the cat: Interindividual variability in retinotopic arrangement and cortical location. *J. Physiol. (Lond.)* 299:247-276.
- Allman, J.M., and J.H. Kaas (1971a) A representation of the visual field in the caudal third of the middle temporal gyrus of the owl monkey (*Aotus trivirgatus*). *Brain Res.* 31:85-105.
- Allman, J.M., and J.H. Kaas (1971b) Representation of the visual field in striate and adjoining cortex of the owl monkey (*Aotus trivirgatus*). *Brain Res.* 39:89-106.
- Allman, J.M., and J.H. Kaas (1974) The organization of the second visual area (V-II) in the owl monkey: A second-order transformation of the visual hemifield. *Brain Res.* 76:247-265.
- Calford, M.B., M.L. Graydon, M.F. Huerta, J.L. Kaas, and J.D. Pettigrew (1985) A variant of the mammalian somatotopic map in a bat. *Nature* 313:477-479.
- Choudhury, B.P. (1978) Retinotopic organization of the guinea pig's visual cortex. *Brain Res.* 144:19-29.
- Clarke, P.G.H., and D. Whitteridge (1976) The cortical visual areas of the sheep. *J. Physiol. (Lond.)* 256:497-508.
- Cotter, J.R. (1981) Retinofugal projections of an echolocating megachiropteran. *Am. J. Anat.* 160:159-174.
- Cotter, J.R. (1985) Retinofugal projections of the big brown bat, *Eptesicus fuscus*, and the neotropical fruit bat, *Artibeus jamaicensis*. *Am. J. Anat.* 172:222-231.
- Cotter, J.R., and R.J.P. Pentney (1979) Retinofugal projections of nonecholocating (*Pteropus giganteus*) and echolocating (*Myotis lucifugus*) bats. *J. Comp. Neurol.* 184:381-400.
- Covey, E., and Casseday, J.H. (1991) The ventral lateral lemniscus in an echolocating bat: Parallel pathways for analyzing temporal features of sound. *J. Neurosci.* 11:3456-3470.
- Daniel, P.M., and D. Whitteridge (1961) The representation of the visual field on the cerebral cortex in monkeys. *J. Physiol. (Lond.)* 159:203-221.
- Dann, J.F., and Buhl, E.H. (1990) Morphology of retinal ganglion cells in the flying fox (*Pteropus scapulatus*): A lucifer yellow investigation. *J. Comp. Neurol.* 301:401-416.
- Drager, U. (1975) Receptive fields of single cells and topography of mouse visual cortex. *J. Comp. Neurol.* 160:269-290.
- Dow, B.M., A.Z. Snyder, R.G. Snyder, and R. Bauer (1981) Magnification factor and receptive field size in foveal striate cortex of the monkey. *Exp. Brain Res.* 44:213-228.
- Fiorani, M., Jr., R. Gattass, M.G.P. Rosa, and A.P.B. Sousa (1989) Visual area MT in the *Cebus* monkey: Location, visuotopic organization and variability. *J. Comp. Neurol.* 287:98-118.
- Florence, S.L., and J.H. Kaas (1992) Ocular dominance columns in area 17 of Old World macaque and talapoin monkeys: Complete reconstructions and quantitative analyses. *Visual Neurosci.* 8:449-462.
- Gallyas, F. (1979) Silver staining of myelin by means of physical development. *Neurol. Res.* 1:203-209.
- Gattass, M., and R. Gattass (1975) Algorithms for the conversion of coordinates of the representation of the visual field. *An. Acad. Bras. Cienc.* 47:317 (in Portuguese).
- Gattass, R., C.G. Gross, and J.H. Sandell (1981) Visual topography of V2 in the macaque. *J. Comp. Neurol.* 201:519-530.
- Gattass, R., A.P.B. Sousa, and M.G.P. Rosa (1987) Visual topography of V1 in the *Cebus* monkey. *J. Comp. Neurol.* 259:529-548.
- Gattass, R., M.G.P. Rosa, A.P.B. Sousa, M.C.G. Pinon, M. Fiorani, Jr., and S. Neuenschwander (1990) Cortical streams of visual information processing in primates. *Braz. J. Med. Biol. Res.* 23:375-393.
- Graydon, M.L., P.P. Giorgi, and J.D. Pettigrew (1987) Vision in flying foxes (Chiroptera: Pteropodidae). *Aust. Mammal.* 10:101-106.

- Hall, W.C., J.H. Kaas, H. Killackey, and I.T. Diamond (1971) Cortical visual areas in the grey squirrel (*Sciurus carolinensis*): A correlation between cortical evoked potential maps and architectonic subdivisions. *J. Neurophysiol.* 34:437-457.
- Hokoç, J.N., L.G. Gawryszewski, E. Volchan, and C.E. Rocha-Miranda (1992) The retinal distribution of ganglion cells with crossed and uncrossed projections and the visual field representation in the opossum. *An. Acad. Bras. Cienc.* 64:293-303.
- Hubel, D.H., and T.N. Wiesel (1974) Uniformity of monkey striate cortex: A parallel relationship between field size, scatter, and magnification factor. *J. Comp. Neurol.* 158:295-306.
- Hughes, A. (1971) Topographical relationships between the anatomy and physiology of the rabbit visual system. *Doc. Ophthalmol.* 30:33-159.
- Hughes, A. (1976) A supplement to the cat schematic eye. *Vision Res.* 16:149-154.
- Hughes, A. (1977) The topography of vision in mammals of contrasting life style: Comparative optics and retinal organization. In F. Crescitelli (ed): *Handbook of Sensory Physiology*, Vol. VII/5, The Visual System in Vertebrates. Berlin: Springer, pp. 613-756.
- Kaas, J.H., W.C. Hall, and I.T. Diamond (1970) Cortical visual areas I and II in the hedgehog: Evoked potential maps and architectonic subdivisions. *J. Neurophysiol.* 33:595-615.
- Kaas, J.H., W.C. Hall, H. Killackey, and I.T. Diamond (1972) Visual cortex of the tree shrew (*Tupaia glis*): Architectonic subdivisions and representation of the visual field. *Brain Res.* 42:491-496.
- Kaas, J.H., L.A. Krubitzer, and K.L. Johanson (1989) Cortical connections of areas 17 (V-I) and 18 (V-II) of squirrels. *J. Comp. Neurol.* 281:426-446.
- Kennedy, H., K.A.C. Martin, G.A. Orban, and D. Whitteridge (1985) Receptive field properties of neurones in visual area 1 and visual area 2 in the baboon. *Neuroscience* 14:405-415.
- Kennedy, W. (1991) Origins of the corticospinal tract in the flying fox: Correlation with cytoarchitecture and electrophysiology. Masters Thesis, University of Queensland.
- Krubitzer, L.A. (1989) Cortical connections of MT in primates. PhD Thesis, Vanderbilt University, Nashville.
- Krubitzer, L.A., and M.B. Calford (1992) Five topographically organized fields in the somatosensory cortex of the flying fox: Microelectrode maps, myeloarchitecture, and cortical modules. *J. Comp. Neurol.* 317:1-30.
- Krubitzer, L.A., M.B. Calford, and L.M. Schmid (1993) Connections of somatosensory cortex in megachiropteran bats: The evolution of complex sensory systems in mammals. *J. Comp. Neurol.*, 327:473-506.
- Law, M.I., K.R. Zahs, and M.P. Stryker (1988) Organization of the primary visual cortex (area 17) in the ferret. *J. Comp. Neurol.* 278:157-180.
- Maguire, W.M., and J.S. Baizer (1984) Visuotopic organization of the prelunate gyrus in rhesus monkey. *J. Neurosci.* 4:1690-1704.
- Maunsell, J.H.R., and Van Essen, D.C. (1987) Topographic organization of the middle temporal visual area in the macaque monkey: Representational biases and the relationship to callosal connections and myeloarchitectonic boundaries. *J. Comp. Neurol.* 266:535-555.
- McConnell, S.K., and S. LeVay (1986) Anatomical organization of the visual system of the mink, *Mustela vison*. *J. Comp. Neurol.* 250:109-132.
- McIlwain, J.L. (1976) Large receptive fields and spatial transformations in the visual system. *Int. Rev. Physiol.* 10:223-249.
- Montero, V.M., A. Rojas, and F. Torrealba (1973) Retinotopic organization of striate and prestriate visual cortex in the albino rat. *Brain Res.* 53:202-207.
- Myerson, J., P.B. Manis, F.M. Miezin, and J.M. Allman (1977) Magnification in striate cortex and retinal ganglion cell layer of owl monkey: A quantitative comparison. *Science* 198:851-857.
- Neuweiler, G. (1962) Bau und leistung des flughundauges (*Pteropus giganteus* gig. Brunn.). *Z. Vergl. Physiol.* 46:13-56.
- Neuweiler, G. (1990) Auditory adaptations for prey capture in echolocating bats. *Physiol. Rev.* 70:615-641.
- Novick, A. (1958) Orientation in paleotropical bats. II. Megachiroptera. *J. Exp. Zool.* 137:443-461.
- Nowak, R.M., and S.C. Paradiso (1983) *Walker's Mammals of the World*, 4th Ed. Baltimore: Johns Hopkins University Press.
- Payne, B.R. (1990) Representation of the ipsilateral visual field in the transition zone between areas 17 and 18 of the cat's visual cortex. *Visual Neurosci.* 4:445-474.
- Pentney, R.P., and J.R. Cotter (1981) Organization of the retinofugal fibers to the dorsal lateral geniculate nucleus of *Pteropus giganteus*. *Exp. Brain Res.* 41:427-430.
- Perry, V.H., and A. Cowey (1985) The ganglion cell and cone distributions in the monkey's retina: Implications for central magnification factors. *Vision Res.* 25:1795-1810.
- Pettigrew, J.D. (1979) Comparison of the retinotopic organization of the visual wulst on nocturnal and diurnal raptors, with a note on the evolution of frontal vision. In S.J. Cool and E.L. Smith (eds): *Frontiers of Visual Science*. Berlin: Springer-Verlag, pp. 328-335.
- Pettigrew, J.D. (1986) Flying primates? Megabats have the advanced pathway from the eye to midbrain. *Science* 231:1304-1306.
- Pettigrew, J.D. (1991) Wings or brain? Convergent evolution in the origins of bats. *Syst. Zool.* 40:199-216.
- Pettigrew, J.D., B. Dreher, C.S. Hopkins, M.J. McCall, and M. Brown (1988) Peak density and distribution of ganglion cells in the retinae of microchiropteran bats: Implications for visual acuity. *Brain Behav. Evol.* 32:39-56.
- Pettigrew, J.D., B.G.M. Jamieson, S.K. Robson, L.S. Hall, K.I. McAnally, and H.M. Cooper (1989) Phylogenetic relations between microbats, megabats and primates (Mammalia: Chiroptera and Primates). *Philos. Trans. R. Soc. Lond. [Biol.]* 325:489-559.
- Picanço-Diniz, C.W. (1987) Organização do sistema visual de roedores da Amazônia: Topografia das áreas visuais da cutia. PhD Thesis, Federal University of Rio de Janeiro.
- Picanço-Diniz, C.W., L.C.L. Silveira, M.P.S. de Carvalho, and E. Oswaldo-Cruz (1991) Contralateral visual field representation in area 17 of the cerebral cortex of the agouti: A comparison between the cortical magnification factor and retinal ganglion cell distribution. *Neuroscience* 44:325-333.
- Reimer, K. (1989) Retinofugal projections in the rufous horseshoe bat, *Rhinolophus rouxi*. *Anat. Embryol. (Berl.)* 180:89-98.
- Rosa, M.G.P., R. Gattass, and M. Fiorani Jr. (1988a) Complete pattern of ocular dominance stripes in V1 of a New World monkey, *Cebus apella*. *Exp. Brain Res.* 72:645-648.
- Rosa, M.G.P., A.P.B. Sousa, and R. Gattass (1988b) Representation of the visual field in the second visual area in the *Cebus* monkey. *J. Comp. Neurol.* 275:326-345.
- Rosa, M.G.P., R. Gattass, and J.G.M. Soares (1991) A quantitative analysis of cytochrome oxidase-rich patches in the primary visual cortex of *Cebus* monkeys: Topographic distribution and effects of late monocular enucleation. *Exp. Brain Res.* 84:195-209.
- Rosa, M.G.P., R. Gattass, M. Fiorani, Jr., and J.G.M. Soares (1992a) Laminar, columnar and topographic aspects of ocular dominance in the primary visual cortex of *Cebus* monkeys. *Exp. Brain Res.* 88:249-264.
- Rosa, M.G.P., L.M. Schmid, L.A. Krubitzer, and J.D. Pettigrew (1992b) Axes of reference for the study of the visual system and visual topography of striate cortex (V1) in the megachiropteran bat, *Pteropus*. *Soc. Neurosci. Abstr.* 18:296.
- Sanides, F., and J. Hoffmann (1969) Cyto- and myeloarchitecture of the visual cortex of the cat and the surrounding integration cortices. *J. Hirnforsch.* 1:79-104.
- Schein, S.J., and F.M. de Monasterio (1987) Mapping of retinal and geniculate neurons onto striate cortex of macaque. *J. Neurosci.* 7:996-1009.
- Silveira, L.C.L., C.W. Picanço-Diniz, L.F.S. Sampaio, and E. Oswaldo-Cruz (1989) Retinal ganglion cell distribution in the *Cebus* monkey: A comparison with the cortical magnification factors. *Vision Res.* 29:1471-1483.
- Sousa, A.P.B., R. Gattass, J.N. Hokoç, and E. Oswaldo-Cruz (1978a) The visual field of the opossum. In C.E. Rocha-Miranda and R. Lent (eds): *Opossum Neurobiology*. Rio de Janeiro: Academia Brasileira de Ciências, pp. 51-65.
- Sousa, A.P.B., R. Gattass, and E. Oswaldo-Cruz (1978b) The projection of the opossum's visual field on the cerebral cortex. *J. Comp. Neurol.* 177:569-588.
- Suga, N. (1989) Principles of auditory information-processing derived from neuroethology. *J. Exp. Biol.* 146:277-286.
- Thiele, A., M. Vogelsang, and K.P. Hoffmann (1991) Pattern of retinotectal projection in the megachiropteran bat *Rousettus aegyptiacus*. *J. Comp. Neurol.* 314:671-683.
- Thompson, J.M., C.N. Woolsey, and S.A. Talbot (1950) Visual areas I and II of cerebral cortex of rabbit. *J. Neurophysiol.* 13:277-288.
- Tiao, Y.-C., and C. Blakemore (1978) Functional organization in the visual cortex of the golden hamster. *J. Comp. Neurol.* 168:459-482.

- Tootell, R.B.H., S.L. Hamilton, and M.S. Silverman (1985) Topography of cytochrome oxidase activity in owl monkey cortex. *J. Neurosci.* 5:2786–2800.
- Tootell, R.B.H., E. Switkes, M.S. Silverman, and S.L. Hamilton (1988) Functional anatomy of macaque striate cortex. II. Retinotopic organization. *J. Neurosci.* 8:1531–1568.
- Tusa, R.J., L.A. Palmer, and A.C. Rosenquist (1978) The retinotopic organization of area 17 (striate cortex) in the cat. *J. Comp. Neurol.* 177:213–236.
- Van Essen, D.C., and J.H.R. Maunsell (1980) Two-dimensional maps of cerebral cortex. *J. Comp. Neurol.* 191:255–281.
- Van Essen, D.C., W.T. Newsome, and J.H.R. Maunsell (1984) The visual field representation in striate cortex of the macaque monkey: Asymmetries, anisotropies and individual variability. *Vision Res.* 24:429–448.
- Van Essen, D.C., D.J. Felleman, E.A. DeYoe, J. Olavarria, and J. Knierim (1990) Modular and hierarchical organization of extrastriate visual cortex in the macaque monkey. *Cold Spring Harbor Symp. Quant. Biol.* 55:679–696.
- Volchan, E., R.F. Bernardes, C.E. Rocha-Miranda, L. Gleiser, and L.G. Gawryszewski (1988) The ipsilateral field representation in the striate cortex of the opossum. *Exp. Brain Res.* 73:297–314.
- Wagor, E., N.J. Mangini, and A.L. Pearlman (1980) Retinotopic organization of striate and extrastriate visual cortex in the mouse. *J. Comp. Neurol.* 193:187–202.
- Wassle, H., U. Grunert, J. Rohrenbeck, and B.B. Boycott (1989) Cortical magnification factor and the ganglion cell density of the primate retina. *Nature* 341:643–646.
- Wimsatt, W.A. (1970) *Biology of Bats*. New York: Academic Press.
- Wise, L.Z., J.D. Pettigrew, and M.B. Calford (1985) Somatosensory cortical representation in the Australian ghost bat, *Macroderma gigas*. *J. Comp. Neurol.* 248:257–262.
- Wong-Riley, M. (1979) Changes in the visual system of monocularly sutured or enucleated cats demonstrable with cytochrome oxidase histochemistry. *Brain Res.* 171:11–28.
- Woolsey, C.N., W.H. Marshall, and P. Bard (1942) Representation of cutaneous tactile sensibility in the cerebral cortex of the monkey as indicated by evoked potentials. *Johns Hopkins Hosp. Bull.* 70:399–441.